Electronic Supplementary Material (ESI) for Inorganic Chemistry Frontiers.

SUPPORTING INFORMATION

Non-precious metal high-entropy alloy with d-d electron interaction for efficient and robust hydrogen oxidation reaction in alkaline media

Jin−Tao Ren, Lei Chen, Hao−Yu Wang, and Zhong−Yong Yuan*

School of Materials Science and Engineering, Smart Sensing Interdisciplinary Science Center, Key Laboratory of Advanced Energy Materials Chemistry (Ministry of Education), Nankai University, Tianjin 300350, China

* Corresponding author. zyyuan@nankai.edu.cn

1. Experimental section

Synthesis of FeCoNiMoW HEA nanoparticles supported on HPC

Typically, 0.5 mmol of $FeCl_3 \cdot 6H_2O$, 0.5 mmol of $CoCl_2 \cdot 6H_2O$, 0.5 mmol of $NiCl_2 \cdot 6H_2O$, 0.5 mmol of $MoCl_5$, 0.5 mmol of WCl_6, 20 mmol of 2-methylimidazole, and 1.5 g of polyacrylonitrile (PAN) were added into a 45 mL stainless steel grinding jar with many steel beads. The mixture was then grounding for 180 min in a Retsch MM400 grinder mill operating at 30 Hz. The resultant products were collected. For the carbonization process, the mixture was heated to 300 °C in Ar with a heating rate of 2 °C min^{-1} and maintained for 3 h. Then, the furnace was heated to 900 °C under 10% H_2/Ar atmosphere and maintained for 3 h. Finally, the as-synthesized FeCoNiMoW HEA/HPC was obtained after the furnace cooling down to room temperature under Ar atmosphere.

Synthesis of metal alloy nanoparticles supported on HPC

Ni/HPC, FeCoNi/HPC, FeCoNiMo/HPC, and FeCoNiW/HPC were also synthesized through the same processes with those of FeCoNiMoW HEA/HPC. The precursor solutions of above control samples contained 2.5 mmol of metal salts with same ratio, 20 mmol of 2-methylimidazole, and 1.5 g of PAN.

Materials characterizations

X-ray diffraction (XRD) patterns were recorded on a Rigaku Smart Lab 3kW diffractometer using Cu *K*α (λ = 1.5418 Å) radiation. Scanning electron microscopy (SEM) images were obtained on a Jeol JSM−7800F microscope. Transmission electron microscopy (TEM), high-resolution transmission electron microscopy (HRTEM), and energy-dispersive X-ray spectroscopy (EDX) were acquired with a Jeol JEM-2800 electron microscope operating at 200 kV. X-ray photoelectron spectroscopy (XPS) was conducted on Thermo Scientific ESCALAB 250Xi with Al *Kα* X−ray source (1486.6 eV). The C 1speak (284.8 eV) was used as the reference standard for the binding energy. Raman spectroscopy was performed on a RTS-HiR-AM spectrometer with laser excitation at 520 nm wavelength.

Electrochemical measurements

A standard three-electrode cell system along with an electrochemical workstation (CHI mosdel 760E) was applied for all the electrochemical measurements. A graphite rod was used as the counter electrode and a Hg/HgO electrode was used as the reference electrode in alkaline media. The Hg/HgO reference electrode was calibrated to a homemade reversible hydrogen electrode. During the electrochemical measurements, the working electrode was prepared by coating the electrocatalyst on a glassy carbon electrode (GCE, 5 mm in diameter). First, the electrocatalyst powders (5 mg) were dispersed in a mixed solution containing deionized water (245 μL), isopropanol (735 μL), and Nafion solution (5 wt%, 20 μL).

Then, the homogeneous electrocatalyst ink (10 μL) was dropped onto the GCE surface and dried to obtain the working electrode. For HOR test, LSV was performed in H_2-saturated 0.1 M KOH solution at a scan rate of 1.0 mV s^{-1}. The GCE coated with electrocatalyst of 0.25 $mg_{catalyst}$ cm^{-2} was used for durability tests in H_2-saturated 0.1 M KOH solution, and chronoamperometry test was performed at a rotation speed of 1600 rpm. To evaluate the resistance to CO poisoning of different catalysts, the working electrode with the mass loading of 0.25 $mg_{catalyst}$ cm^{-2} on GCE was evaluated *via* chronoamperometry test at 0.1 V vs. RHE in H_2/1000 ppm CO-saturated KOH solution (0.1 M).

The specific exchange current density (j_0) which is normalized to the electrode area was obtained by fitting j_k with Butler–Volmer equation.[1,2]

$$j_k = j_0(e^{\frac{\alpha F}{RT}\eta} - e^{\frac{(1-\alpha)F}{RT}\eta})$$

where j_0 is the exchange current, α is the charge transfer coefficient, R is the universal gas constant (8.314 J mol^{-1} K^{-1}), T is the temperature (K), α and j_0 are set as variables.

The kinetic current (j_k) was calculated based on the Koutecky–Levich equation.[3]

$$\frac{1}{j} = \frac{1}{j_k} + \frac{1}{j_d} = \frac{1}{j_k} + \frac{1}{BC_0\omega^{1/2}} = \frac{1}{j_k} + \frac{1}{0.62nFD^{2/3}V^{-1/6}C_0\omega^{1/2}}$$

where j stands for the measured current density, j_d represents the diffusion current density, B is the Levich constant, C_0 is the solubility of H_2 (7.33×10^{-4} mol L^{-1}), F is Faraday constant (96 485 C mol^{-1}), D is the H_2 diffusion coefficient in 0.1 M NaOH, v is the kinematic viscosity (1.01×10^{-2} cm^2 s^{-1}), and ω is the rotating rate. j_d can be obtained based on Nernstian diffusion overpotential equation.[1]

$$j_d = j_l(1 - \exp(-\frac{2F\eta}{RT}))$$

where j_l is the diffusion-limited current, η represents the overpotential.

DFT Calculations

First-principles computations on basis of DFT were performed with the plane-wave technique as implemented in the Vienna ab initio simulation package (VASP).[4,5] The projector augmented wave (PAW) pseudopotential was utilized and a 500 eV cutoff was adopted for the plane wave basis set.[6] The generalized gradient approximation (GGA) involving the Perdew, Burke, and Ernzerhof (PBE) functional was used.[7,8] A vacuum space with at least 15 Å was inserted between the surface adsorption model and its periodically repeated images. The k-point sampling of the Brillouin zone was obtained using 2 × 2 × 1 by Monkhorst–Pack scheme. All DFT calculations are to minimize the total energy until the convergence criterion of 10^{-4} eV, and all the residual forces were converged to 0.05 eV $Å^{-1}$. The Brillouin zone is

sampled with a Gamma-centered special k-points grid of 2 × 2 × 1 for geometry optimization. The free energy was calculated on the basis of the computational hydrogen electrode (CHE) model.[9,10]

Adsorption energy ΔE of H atom on the surface of substrates was defined as:

$$\Delta E = E_{*H} - (E_{*} + E_{H})$$

where *H and * denoted the adsorption of H atom on substrates and the bare substrates, E_H denoted the half energy of H_2 gas.

Gibbs free energy change (ΔG) of each chemical reaction was calculated by:

$$\Delta G = \Delta E + \Delta ZPE - T\Delta S$$

where E, ZPE, T and S denote the calculated total energy, zero point energy, temperature and entropy, respectively.

2. Supplementary figures

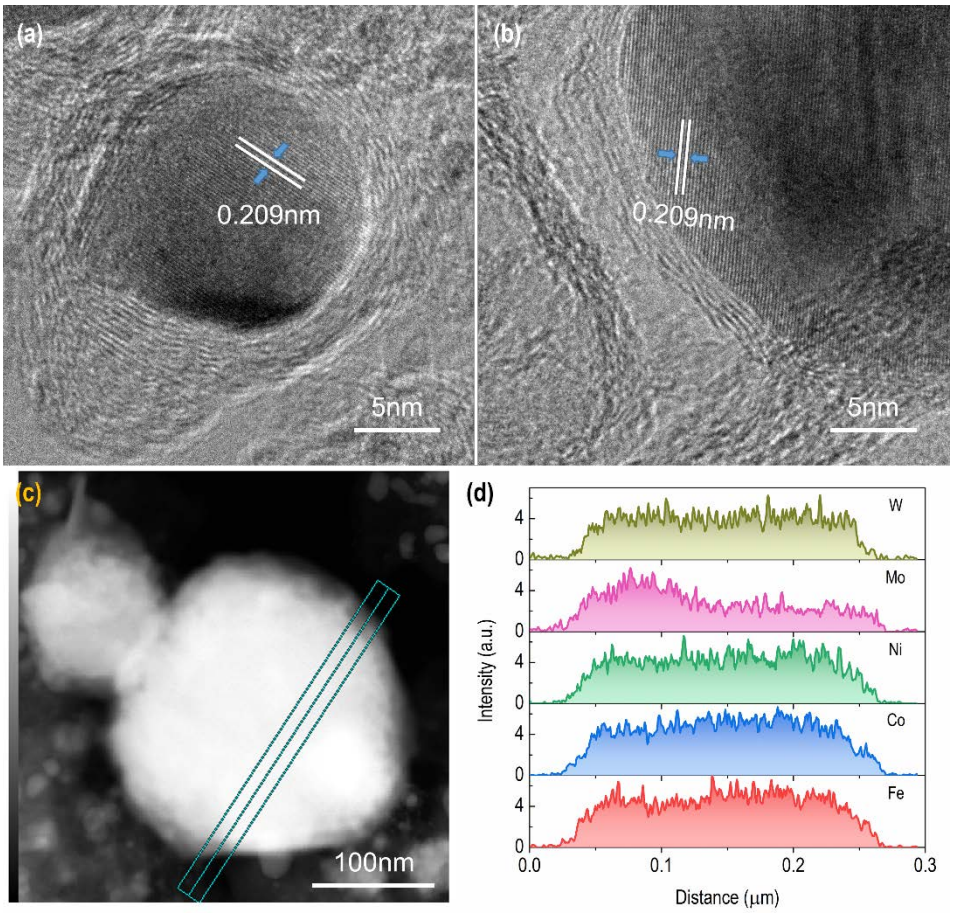

Fig. S1 (a,b) High-resolution TEM images of HEA/HPC. (c,d) Line-scan STEM-EDX spectra of HEA/HPC in the area marked in STEM image.

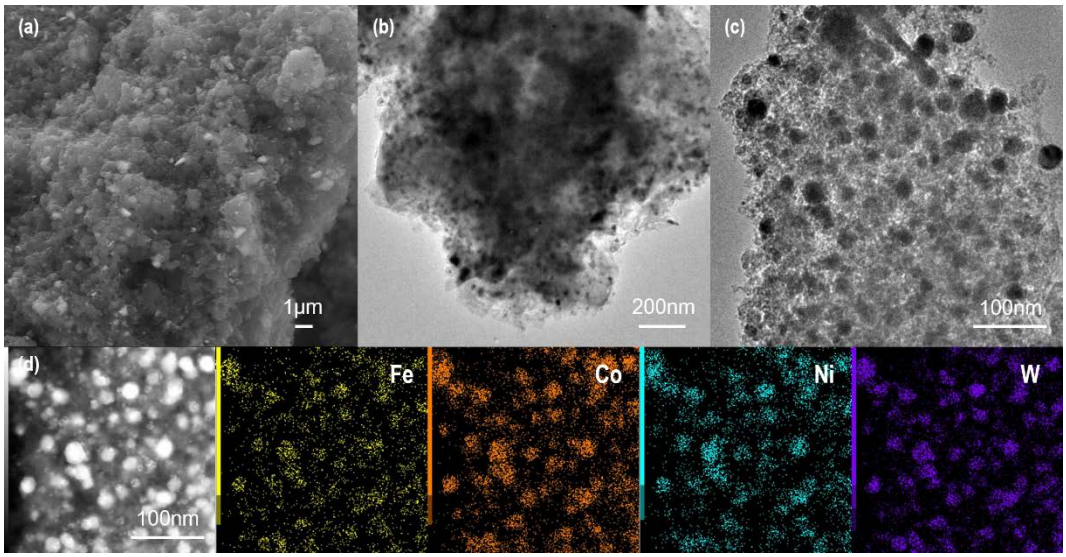

Fig. S2 (a) SEM, and (b,c) TEM images of FeCoNiW/HPC sample. (d) STEM-EDX mapping images of the NPs supported on HPC substrate.

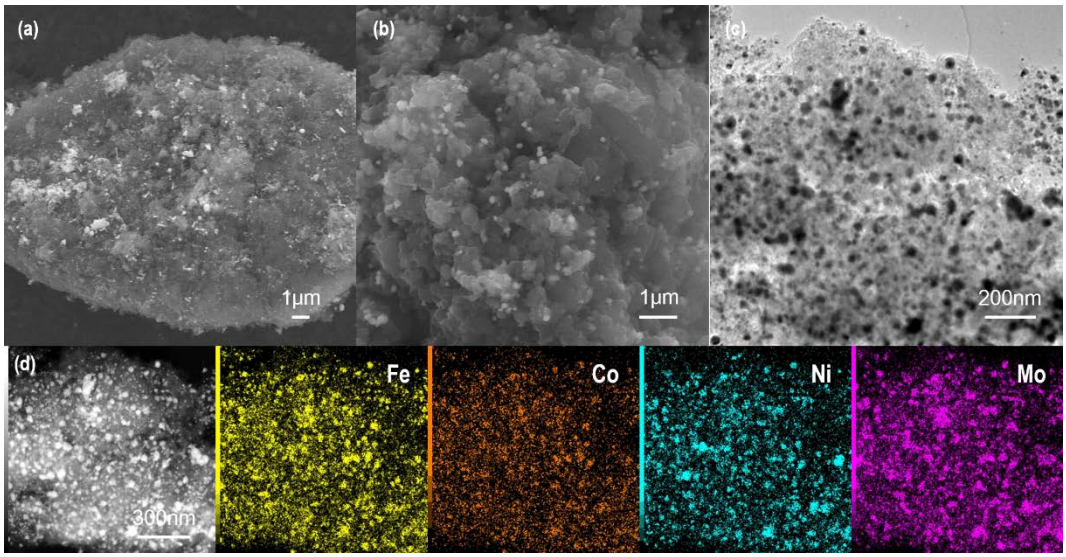

Fig. S3 (a) SEM, and (b,c) TEM images of FeCoNiMo/HPC sample. (d) STEM-EDX mapping images of the NPs supported on HPC substrate.

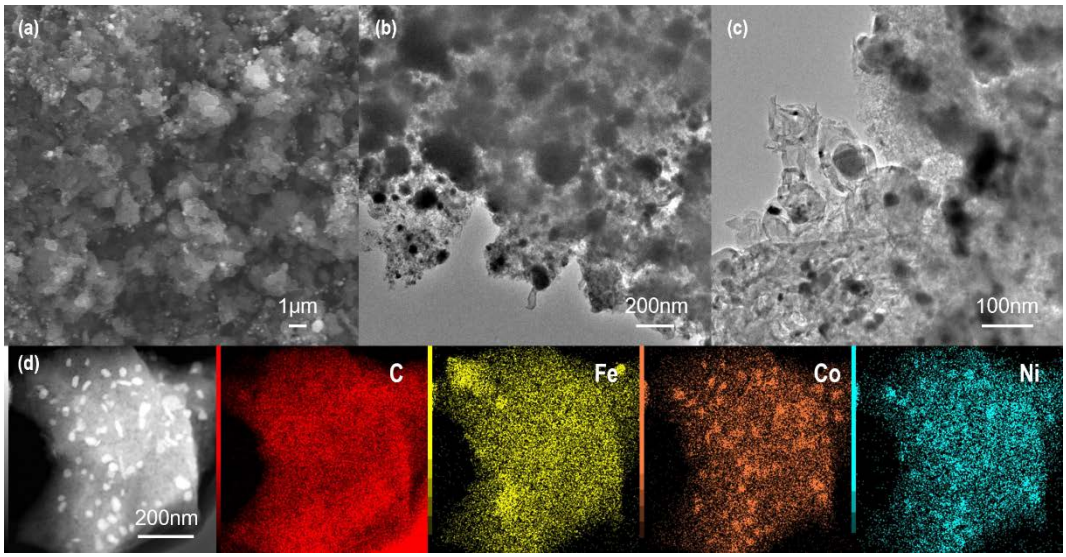

Fig. S4 (a) SEM, and (b,c) TEM images of FeCoNi/HPC sample. (d) STEM-EDX mapping images of the NPs supported on HPC substrate.

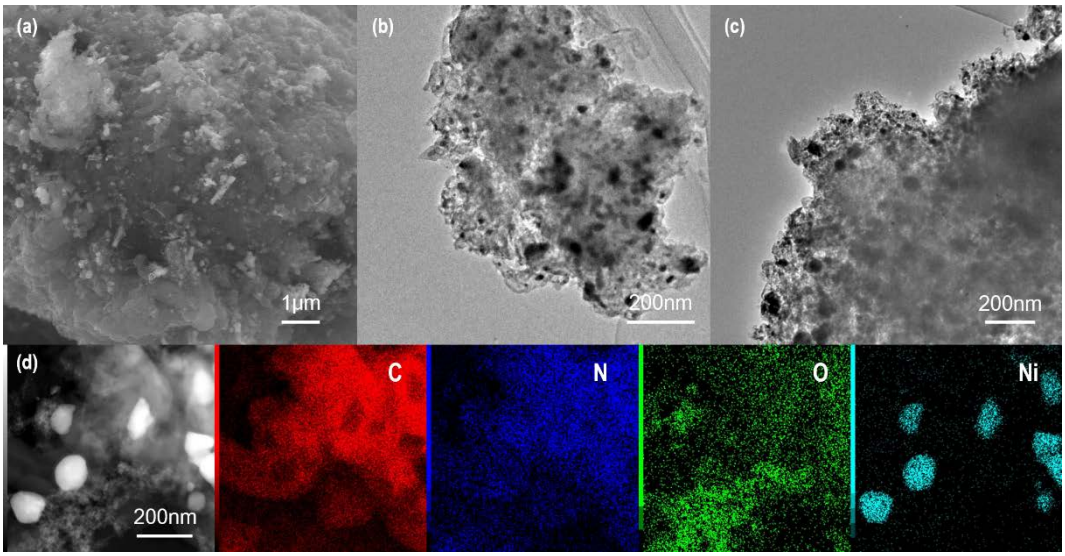

Fig. S5 (a) SEM, and (b,c) TEM images of Ni/HPC sample. (d) STEM-EDX mapping images of the NPs supported on HPC substrate.

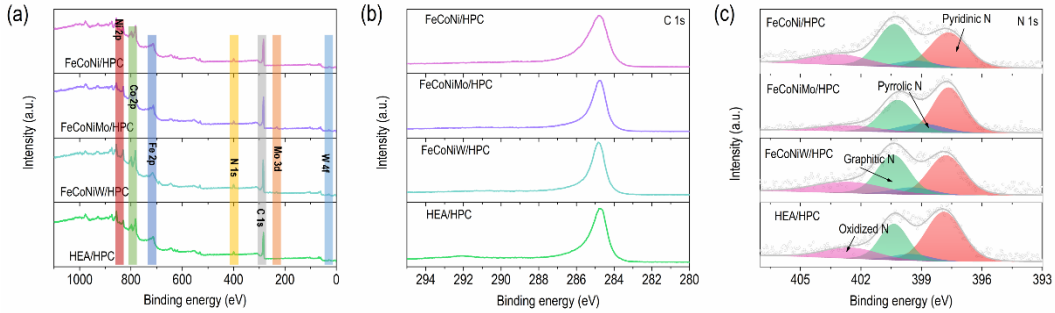

Fig. S6 (a) XPS survey spectra, and high-resolution XPS spectra of C 1s (b) and N 1s (c) of the prepared catalysts.

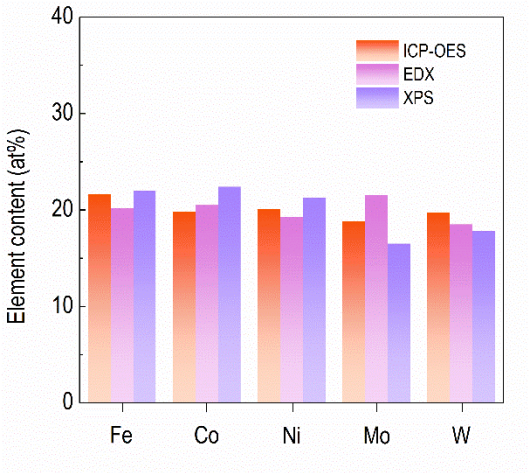

Fig. S7 The overall atomic percentages of metals in the FeCoNiMoW HEA/HPC as determined by ICP-OES, EDX, and XPS spectra. The calculation of mixed entropy for HEAs could be made following the equation: $\Delta S_{mix} = -R\sum_{i=1}^{n} X_i \ln X_i$, where ΔS_{mix} is the configurational entropy of mixing, R is the gas constant, X_{i} is the molar ratio of component i, and n is the total number of elements involved. Therefore, the calculated mixing entropy of ΔS is higher than 1.50 R, illustrating the formation of HEA.

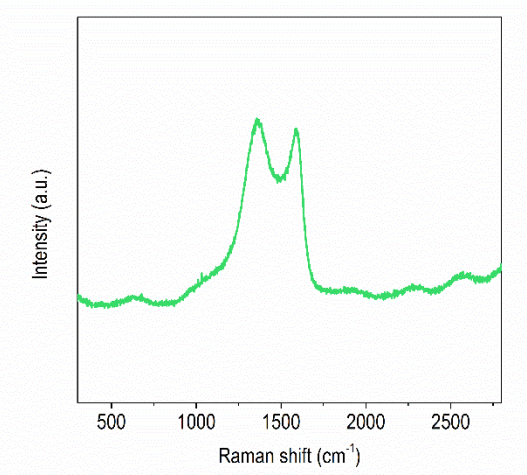

Fig. S8 Raman spectrum of FeCoNiMoW HEA/CNFs.

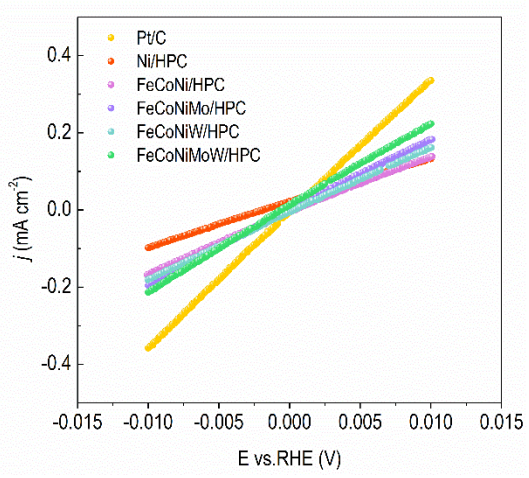

Fig. S9 Linear fitting curves at micropolarization region of HOR/HER.

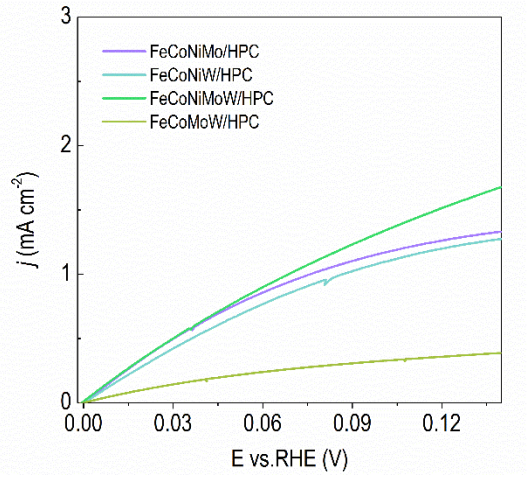

Fig. S10 LSV curves of the as-prepared catalysts in H_2-saturated 0.1 M KOH.

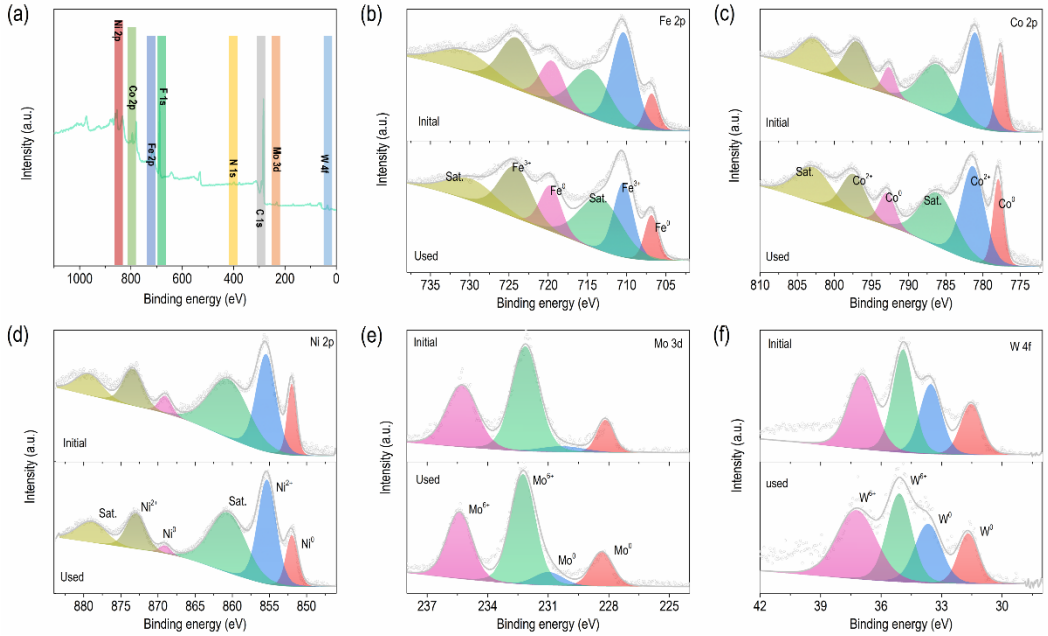

Fig. S11 (a) XPS survey spectra of the HEA/HPC catalyst after HOR test. High-resolution XPS spectra of Fe 2p (b), Co 2p (c), Ni 2p (d), Mo 3d (e), and W 4f (f) core levels for the HEA/HPC catalyst before and after HOR test.

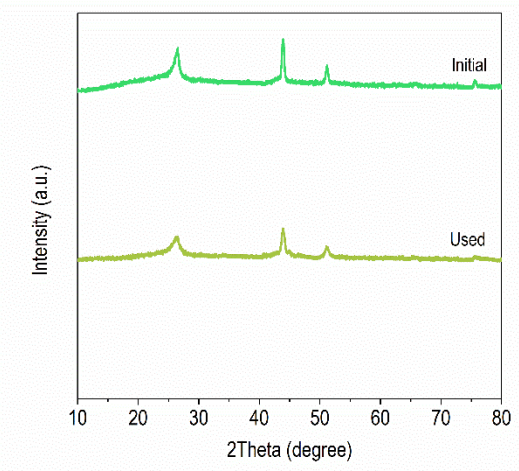

Fig. S12 XRD pattern of HEA/HPC catalyst before and after HOR test.

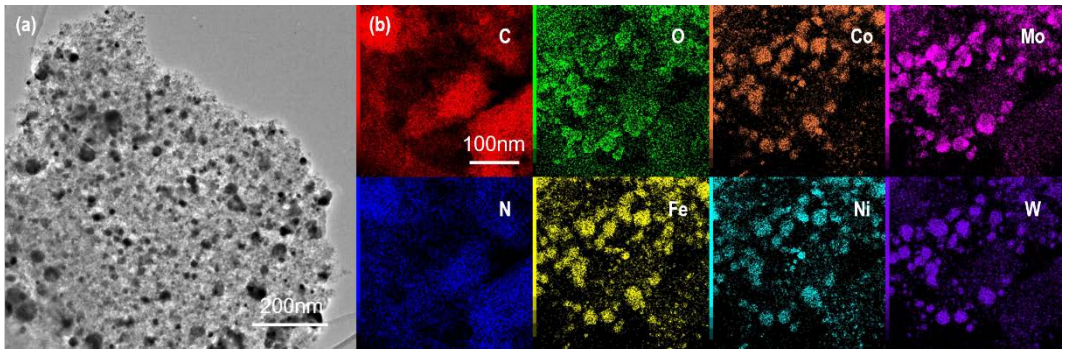

Fig. S13 (a) TEM, and (b) STEM-EDX mapping images of the HEA/HPC catalyst after HOR stability test.

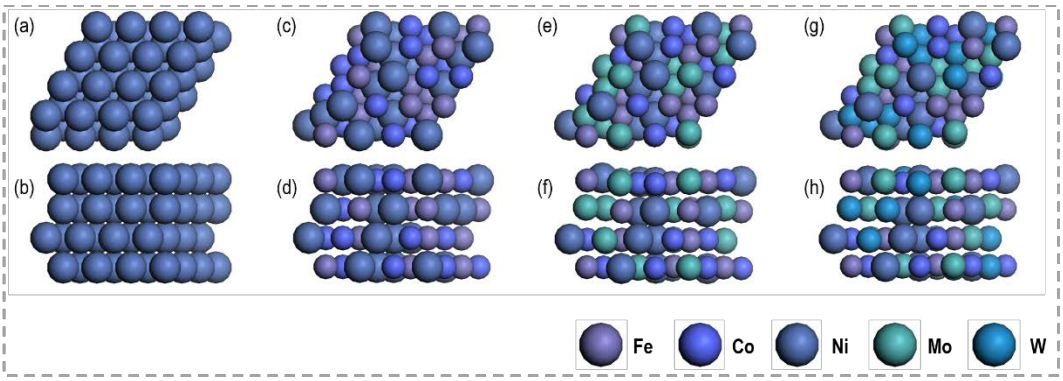

Fig. S14 The top view and side view of the optimized Ni model (a,b), FeCoNi model (c,d), FeCoNiMo model (e,f), and FeCoNiMoW model (g,h).

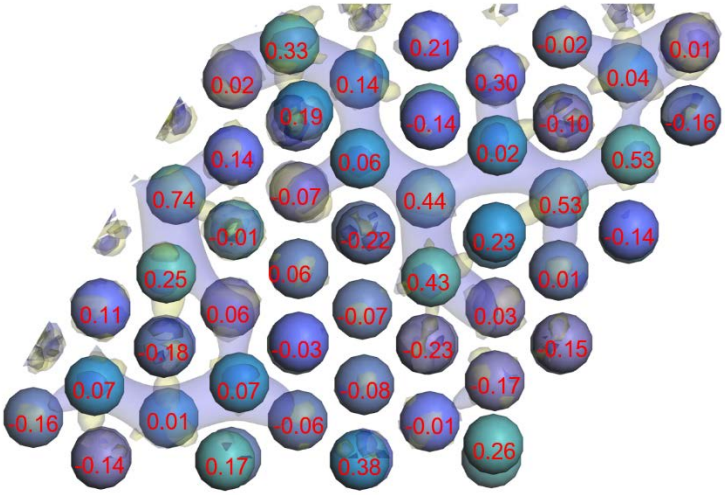

Fig. S15 Charge density difference analysis of FeCoNiMoW.

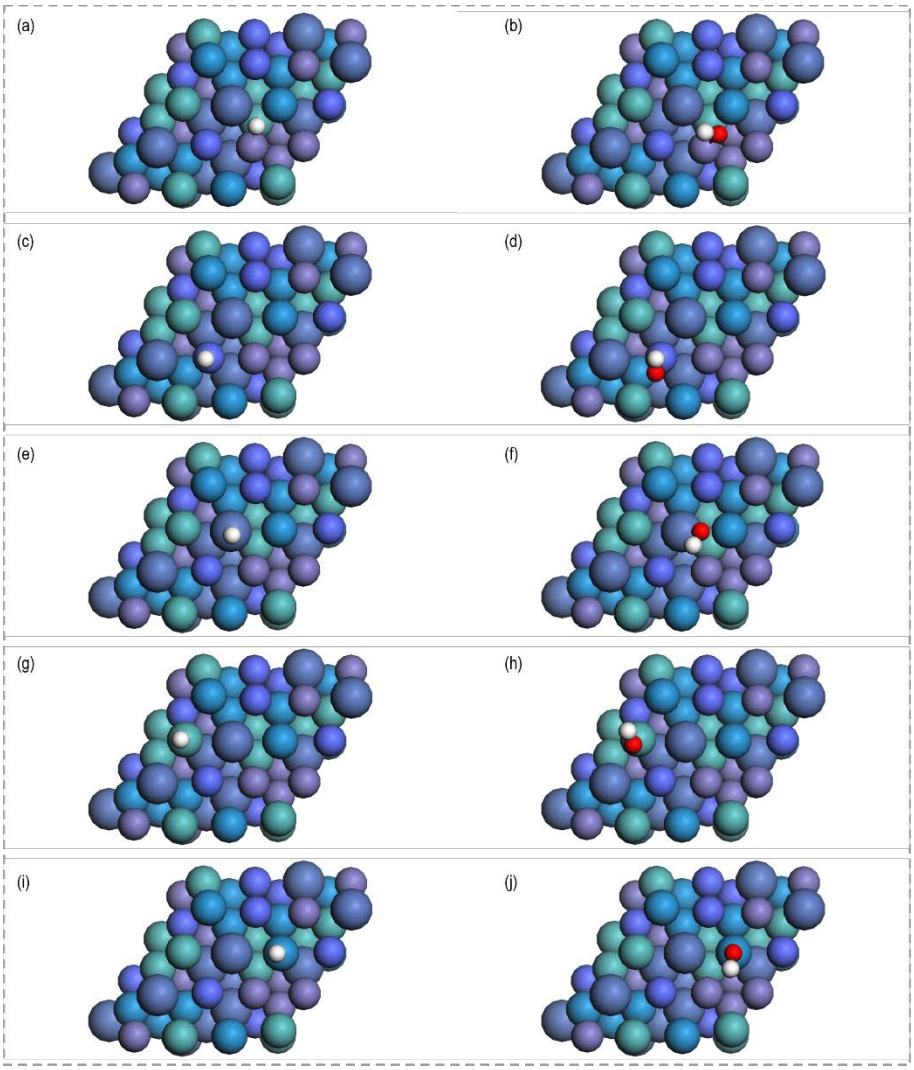

Fig. S16 The adsorption sites of *H and *OH on Fe atom (a,b), Co atom (c,d), Ni atom (e,f), Mo atom (g,h), and W atom (i,j) of FeCoNiMoW slab.

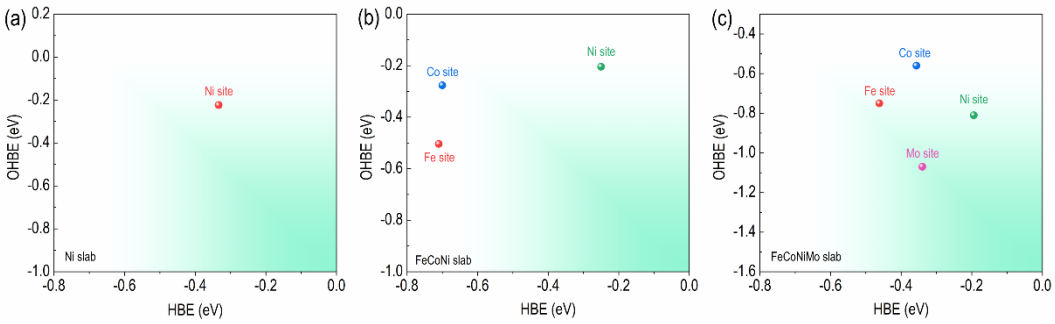

Fig. S17 The calculated HBE and OHBE on different surface metal sites of Ni slab (a), FeCoNi slab (b), and FeCoNiMo slab (c).

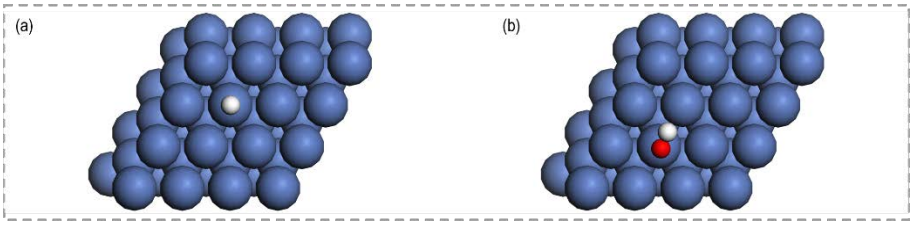

Fig. S18 The adsorption sites of *H (a) and *OH (b) on Ni atom of Ni slab.

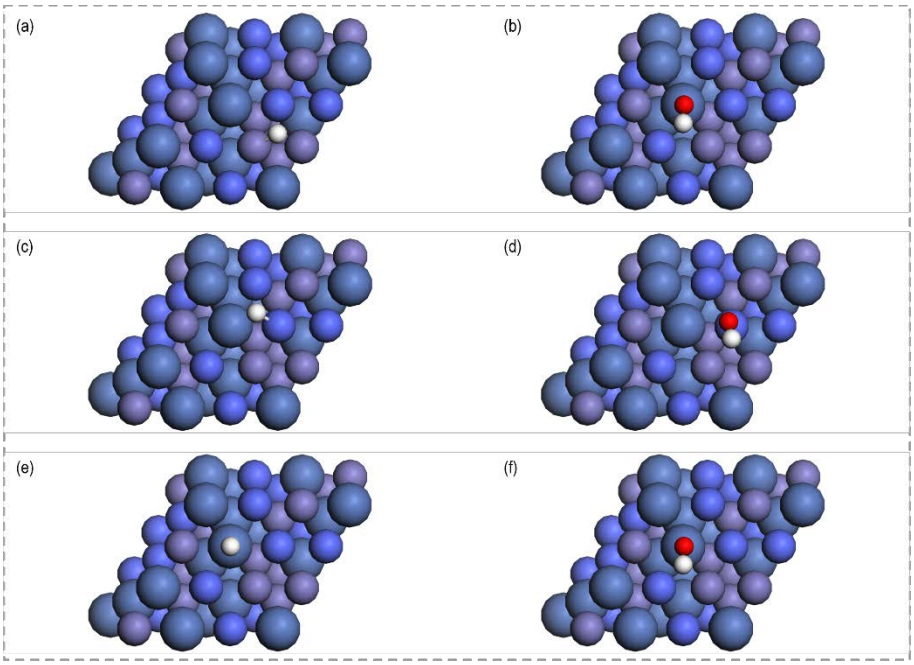

Fig. S19 The adsorption sites of *H and *OH on Fe atom (a,b), Co atom (c,d), and Ni atom (e,f) of FeCoNi slab.

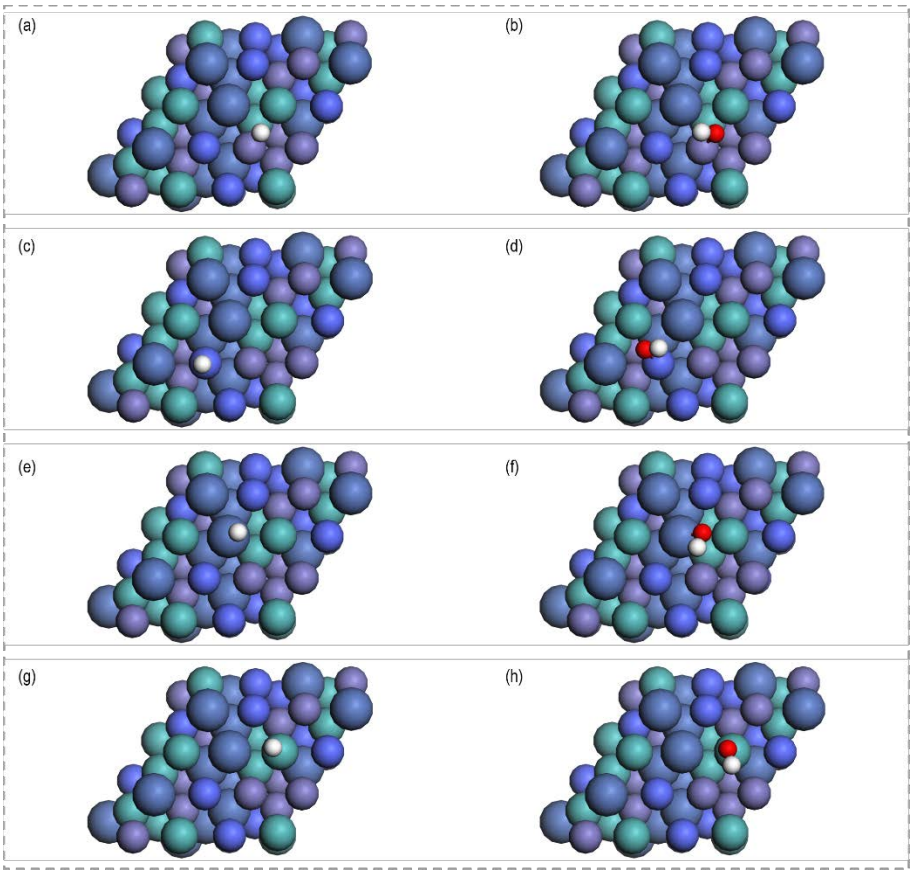

Fig. S20 The adsorption sites of *H and *OH on Fe atom (a,b), Co atom (c,d), Ni atom (e,f), and Mo atom (g,h) of FeCoNiMo slab.

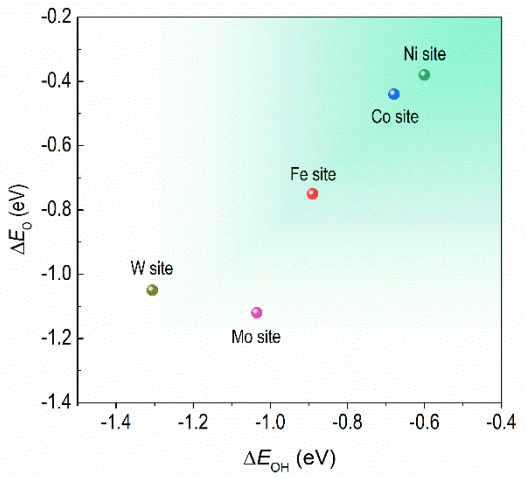

Fig. S21 The calculated OBE and OHBE on different surface metal sites of FeCoNiMoW slab.

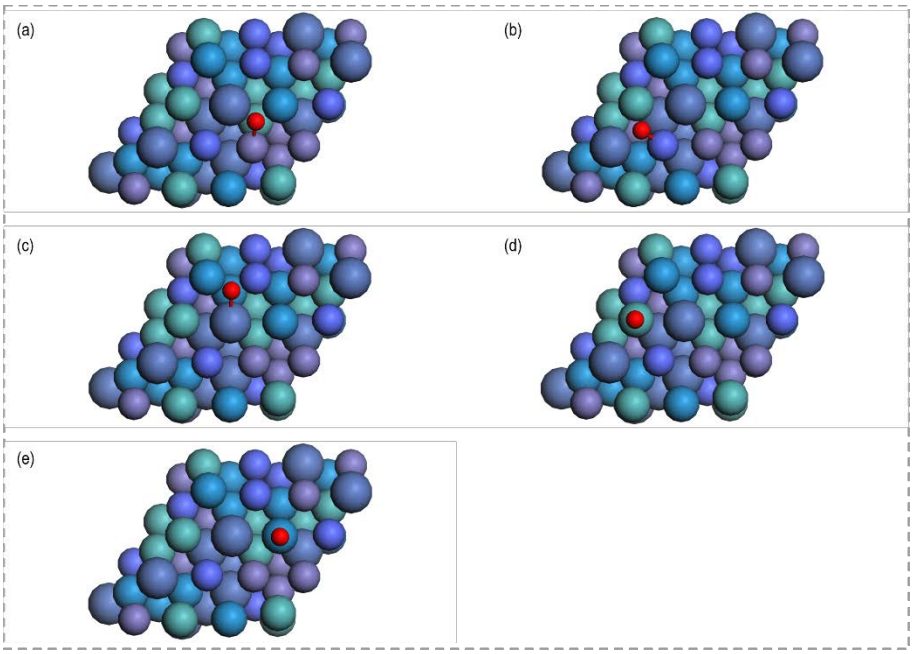

Fig. S22 The adsorption sites of *O on Fe atom (a), Co atom (b), Ni atom (c), Mo atom (d), and W atom (e) of FeCoNiMoW slab.

3. References

1 G. Zhao, L. Xia, P. Cui, Y. Qian, Y. Jiang, Y. Zhao, H. Pan, S. X. Dou and W. Sun, Atomic-Level Modulation of the Interface Chemistry of Platinum–Nickel Oxide toward Enhanced Hydrogen Electrocatalysis Kinetics, *Nano Letters*, 2021, **21**, 4845-4852.

2 G. Wang, J. Parrondo, C. He, Y. Li and V. Ramani, Pt/C/Ni(OH)$_2$ Bi-Functional Electrocatalyst for Enhanced Hydrogen Evolution Reaction Activity under Alkaline Conditions, *Journal of The Electrochemical Society*, 2017, **164**, F1307-F1315.

3 J. Ohyama, T. Sato, Y. Yamamoto, S. Arai and A. Satsuma, Size Specifically High Activity of Ru Nanoparticles for Hydrogen Oxidation Reaction in Alkaline Electrolyte, *Journal of the American Chemical Society*, 2013, **135**, 8016-8021.

4 M. D. Segall, J. D. L. Philip, M. J. Probert, C. J. Pickard, P. J. Hasnip, S. J. Clark and M. C. Payne, First-principles simulation: ideas, illustrations and the CASTEP code, *Journal of Physics: Condensed Matter*, 2002, **14**, 2717.

5 G. Kresse and J. Furthmüller, Efficient iterative schemes for ab initio total-energy calculations using a plane-wave basis set, *Physical Review B*, 1996, **54**, 11169-11186.

6 G. Kresse and D. Joubert, From ultrasoft pseudopotentials to the projector augmented-wave method, *Physical Review B*, 1999, **59**, 1758-1775.

7 J. P. Perdew, K. Burke and M. Ernzerhof, Generalized Gradient Approximation Made Simple, *Physical Review Letters*, 1996, **77**, 3865-3868.

8 B. Hammer, L. B. Hansen and J. K. Nørskov, Improved adsorption energetics within density-functional theory using revised Perdew-Burke-Ernzerhof functionals, *Physical Review B*, 1999, **59**, 7413-7421.

9 V. Viswanathan, H. A. Hansen, J. Rossmeisl and J. K. Nørskov, Unifying the 2e– and 4e– Reduction of Oxygen on Metal Surfaces, *The Journal of Physical Chemistry Letters*, 2012, **3**, 2948-2951.

10 J. K. Nørskov, J. Rossmeisl, A. Logadottir, L. Lindqvist, J. R. Kitchin, T. Bligaard and H. Jónsson, Origin of the Overpotential for Oxygen Reduction at a Fuel-Cell Cathode, *The Journal of Physical Chemistry B*, 2004, **108**, 17886-17892.